6ICEGE 6th International Conference on Earthquake Geotechnical Engineering
1-4 November 2015
Christchurch. New Zealand

Liquefaction-induced lateral spreading in Coronel: Field survey and numerical modeling

G. de la Maza[1], N. Williams[2], E. Sáez[1], K. Rollins[2], C. Ledezma[1]

ABSTRACT

The paper describes a detailed field survey conducted at Lo Rojas fishermen port in Coronel, where extensive liquefaction induced lateral-spreading was reported for the 2010, Mw 8.8 Maule earthquake. The survey includes SPT and CPT soundings, as well as the use of some surface-based geophysical techniques. The data was used to develop a detailed hydro-mechanical finite element model, which results reasonably agree with the post-event field observations.

Introduction

The February 27, 2010 Mw 8.8 Maule earthquake caused important damage to ports and bridges, considerably affecting the country's economic activities. In many cases, this damage was associated with liquefaction-induced lateral spreading phenomena, in which large masses of soil slide over a liquefied layer, imposing large displacement demands on existing structures. Caleta Lo Rojas, located 25 km south of Concepción, is a fishermen's wharf that showed clear evidence of liquefaction-induced lateral spreading. The most damaged structure was a pier, which had to be replaced after the earthquake (Figure 1). The large horizontal displacements that affected the area produced the complete failure of the old pier (Figure 1b). During a post-earthquake reconnaissance (Bray et al., 2012), cumulative horizontal displacements were measured by summing the crack widths along the line indicated in Figure 1a. A lateral maximum movement of about 2.6 m was observed across a distance of approximately 85 m (Figure 1c).

Exploration Boreholes

Boreholes SM-1 and SM-2 were drilled for the new wharf's construction project in 2010, next to the old pier that was severely damaged during the earthquake (Figure 1b). Each borehole had a depth of about 25 meters from the mean sea-level. An additional borehole, ST-1, was drilled in 2014 to a depth of 20 meters from a relative elevation of 2.87 meters above sea-level. Additionally, two Cone Penetration Tests (CPT5 and CPT6) were performed. Boreholes and CPT locations are shown in Figure 1a.

Figure 2a displays the normalized blow count $N_{1,60}$ values. Results from SM-1 and SM-2 were

[1] Structural and Geotechnical Engineering Department, Pontificia Universidad Católica de Chile, Santiago, Chile, gadelama@ing.puc.cl, esaez@ing.puc.cl, ledezma@ing.puc.cl
[2] Department of Civil & Environmental Engineering, Brigham Young University, Provo, USA, nicoledwwilliams@gmail.com, rollinsk@byu.edu

corrected assuming an energy efficiency of 60%, while for ST-1 the energy was recorded during the SPT tests. Using the available bathymetry, absolute vertical elevations to mean sea-level were computed for each borehole. The results show a sharp contrast between the first 20 meters and deeper soils. ST-1 shows that the transition from soft to denser material occurs at about 14 m below sea-level, while the marine soundings indicate that this transition takes place at 20 m below sea-level.

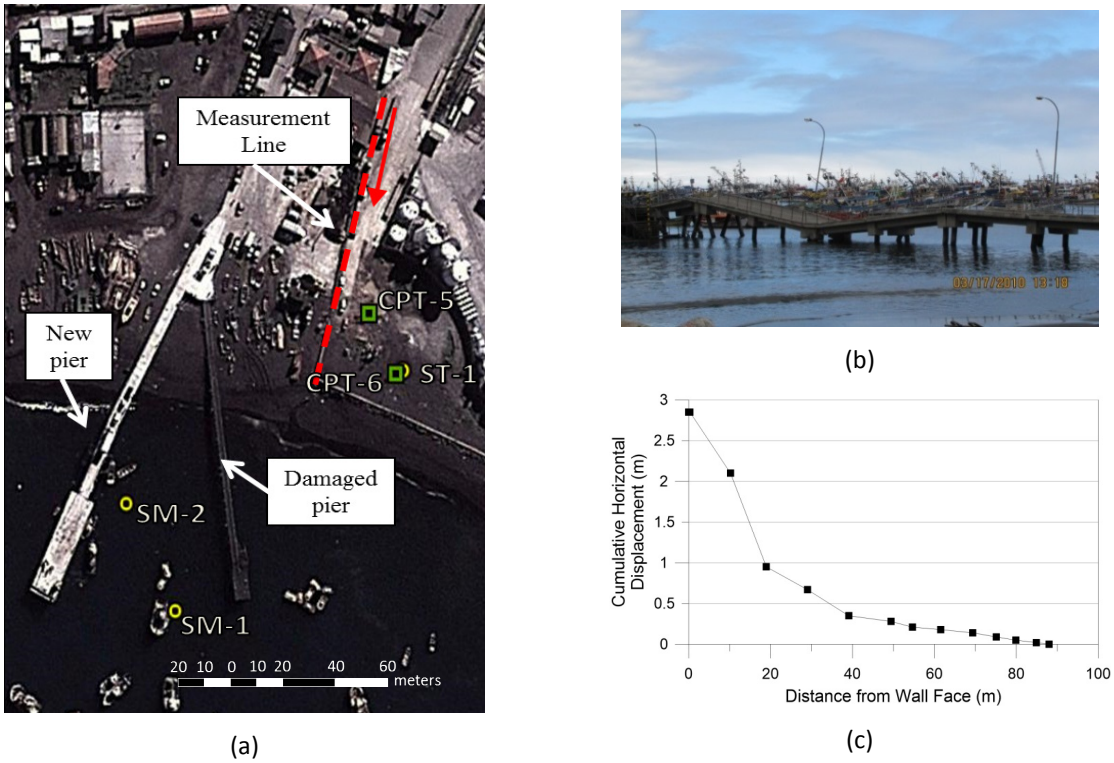

Figure 1. (a) Lateral spread measurement line and location of geotechnical soundings; (b) Damaged pier; (c) Cumulative horizontal ground displacements.

Figure 2c displays SBT (Soil Behavior Type) from CPT borings. The data indicates two dominant materials in the first 20 meters: sand and silt. There is a transition between these two soils as the SBT values show. The upper 8 meters are mainly clean sands that progressively change to silty sand for the following 4 meters, and then turn into clayey silt to silty clay at 20 m below the surface. $N_{1,60}$ values for the first 20 meters are fairly uniform with blow-counts of less than 10 blows/ft. Also, the USCS classification from ST-1 samples (Figure 2a) agrees with the SBT index, showing very similar transitions and designations. With such low values of $N_{1,60}$, conventional liquefaction assessment methods predict liquefaction down to 20 m below sea-level. The Factor of Safety against liquefaction (FSL) was calculated from the SPT and CPT measurements (Figure 2b), considering a peak horizontal acceleration a_{max} = 0.3 (Concepción), a magnitude Mw = 8.8 and fines content corrections (Youd et al, 2001).

Bray and Sancio (2006) proposed limits to define if fines are likely to liquefy or not. According to these authors, if the Plasticity Index (PI) is larger than 20 or the moisture content is lower than 0.8 times the Liquid Limit value, the material is not susceptible to liquefaction. Clay layers CH

and CL (from z = -11 to -19 m) meet at least one of these conditions, probably defining the depth limit for the liquefiable behavior, and the surface above which lateral-spreading takes place.

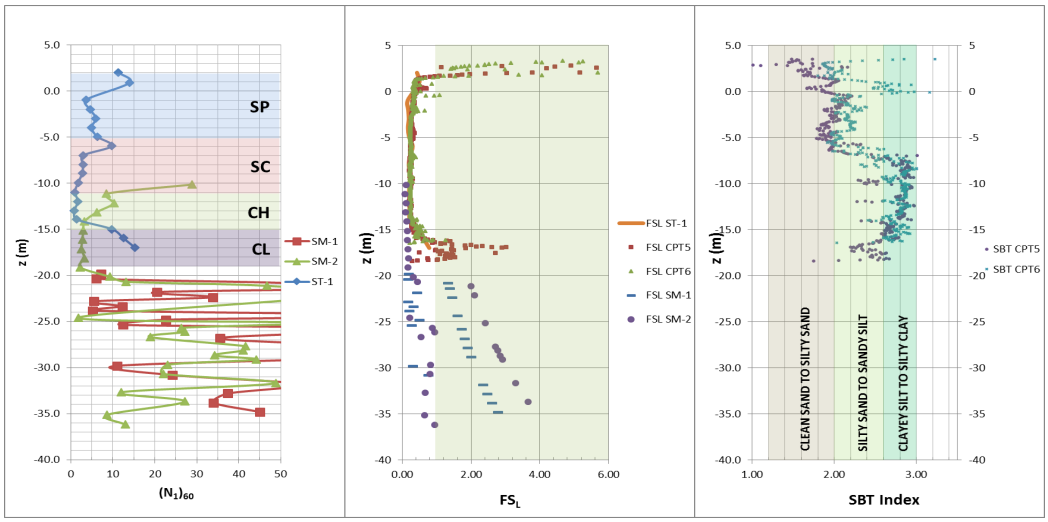

Figure 2. (a) Stratigraphy and comparison from 3 boreholes (SM-1, SM-2 and ST-1); (b) Factor of Safety against liquefaction from CPT soundings; (c) SBT Index from CPT soundings.

Geophysical Survey

The geophysical survey in Caleta Lo Rojas included two areas, labeled SW-1 and SW-2 (Fig. 3). Two different geophone arrays were used on each area. Additionally, the Horizontal to Vertical Spectral Ratio (Nakamura, 1989) was calculated at six points, which are also displayed with circular markers in Figure 3. The marker's colors show the calculated fundamental frequency according to the color scale on the left (in Hertz), while their size shows the peak amplitude, with the corresponding scale on the right side.

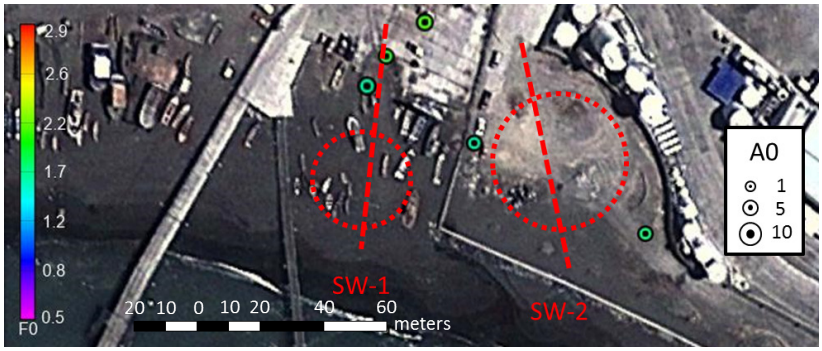

Figure 3. Geophysical survey: Nakamura results and explored area.

Seismic surface-wave based geophysics methods characterize dispersive properties of a site using both, passive sources (ambient vibrations) and active sources (sledgehammer). The analysis performed assumed only Rayleigh waves. For source controlled experiments (active tests), we used the Multichannel Analysis of Surface Waves, MASW, method (Park et al. 1999).

For ambient noise measurements (passive sources), we used SPAC (Aki, 1957) and f-k methods (Lacoss et al., 1969) in the case of bi-dimensional arrays. Additionally, for the analysis of passive linear measurements, we used the Extended SPAC (ESPAC) under the assumption of isotropic incident fields (Hayashi, 2008).

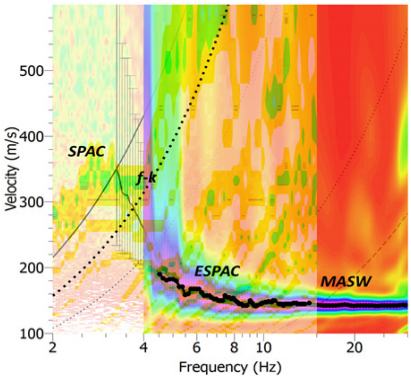

(a)

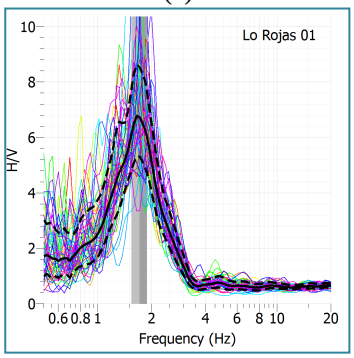

(b)

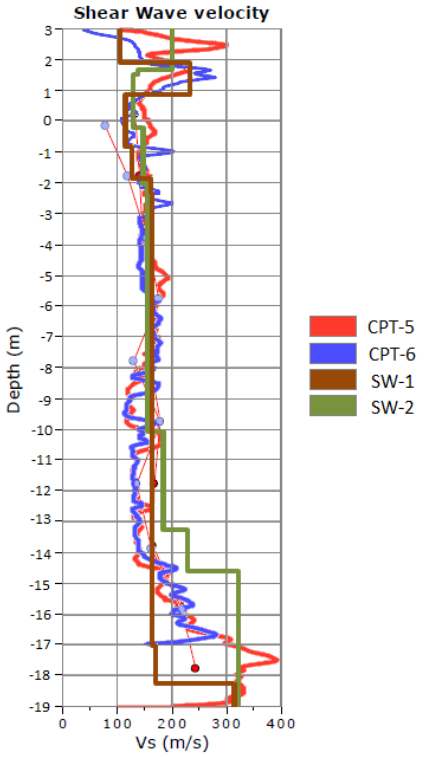

(c)

Figure 4. (a) SW-2 geophysical survey geometry; (b) Example of H/V curve; (c) shear wave profiles (two sites and comparison with CPT).

Figure 4a displays the dispersive properties of the SW-2 area, combining the results of SPAC, f-k, ESPAC and MASW methods along a linear and a circular array. Different techniques are consistent and they allow characterization of the dispersion curve between 2.5 and 30 Hz approximately. In this work, we used the extension of the Neighborhood Algorithm proposed by Wathelet (2008) to solve the inverse problem. The results of the application of this method to areas SW-1 and SW-2 are shown in Figure 4c. The results are compared against “direct” measurements performed with the seismic cone on CPT-5 and CPT-6. The shear wave velocity profiles obtained from the geophysical survey agree well with the profiles obtained from the CPT measurements.

Figure 4b shows a typical result of H/V Spectral Ratio. The large amplitude peak implies the existence of a clear stiffness contrast at a given depth. The mean fundamental frequency for this site is f0 = 1.66 Hz, with a representative shear wave velocity of Vs = 160 m/s. If the well-known formula Vs = 4 H f0 is used, these measurements show that the impedance contrast should be located at a depth of 24 m from the soil surface, which is in good agreement with the depth reported in Figure 4c. Even if this stiffer material detected by Nakamura’s method is not the bedrock, this stiffness contrast defines the predominant vibration period for this site.

Geotechnical Model

To estimate lateral spreading using both empirical and detailed numerical methods, a geotechnical model of the area was built. This model was constructed based on the available bathymetry provided by the Ports Department of the Ministry of Public Works along the cross section displayed in Figure 5a.

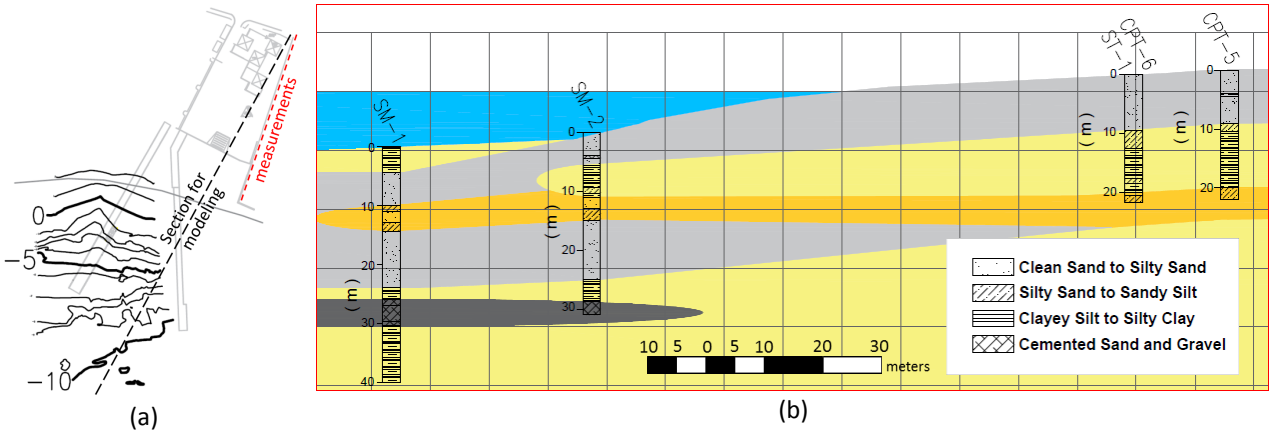

Figure 5. Geotechnical model: (a) Selected section for modeling; (b) Geotechnical model

Although the available borings are not exactly located along the selected section, that section was chosen to take full advantage of the available bathymetry data. The adopted geotechnical model based on boreholes, geophysics, and available bathymetry is shown in Figure 5b. In this figure, each square is 10x10 m. The bathymetry shows a pronounced slope of about 11% close to the coast, a necessary condition to develop lateral spreading. The profile is characterized mainly by three materials: H1 (clean sand to silty sand), H2 (silty sand to sandy silt) and H3 (clayey silt to silty clay). Additionally, a lens of cemented sand and gravel was assumed based on the SM-1 borehole information. Material H1 is liquefiable, while it is not clear if the upper portion of material H2 (somewhere between z = -11m to -15m) may or may not liquefy due to the increase of fines content with depth. H3 is considered to be non-liquefiable. For the sand and silty sand layer (H1), marine borings SM-1 and SM-2 show erratic values of FSL value below z = -20 m (Figure 2b). The material at this depth is probably too dense to liquefy, therefore, for the lateral spreading assessment presented in the next two sections, it was assumed that H1 material located below z = -20 m could not liquefy.

Numerical Modeling

Based on the geotechnical information summarized in Figure 5, we developed a fully coupled hydro-mechanic inelastic finite element model to reproduce the field observations shown in Figure 1c. In this model, the soil-fluid mixture was treated according the u-p formulation (Zienkiewicz and Shiomi, 1984). The construction of a finite element mesh requires limiting the extent of the problem, both horizontally and vertically. Vertically, the model displayed in Figure 6 was extended 5 m below the bedrock, and paraxial elements were used below this level (Modaressi and Benzenati, 1994). The function of these elements is twofold: on one hand they

are used to introduce the earthquake loading to the model after de-convolution from the outcropping bedrock, and on the other, they absorb the waves originating inside the model due to its reflection on the surface and those at the interfaces between layers of soil. The horizontal extension of the model was limited to 260 m. This distance is large enough to capture local effects in the steepest part of the slope. Since the model is completely inelastic, traditional absorbent elements cannot be used on the vertical edges. One way to solve this problem is to use appropriate lateral boundaries to ensure "free-field" conditions far away from the slope.

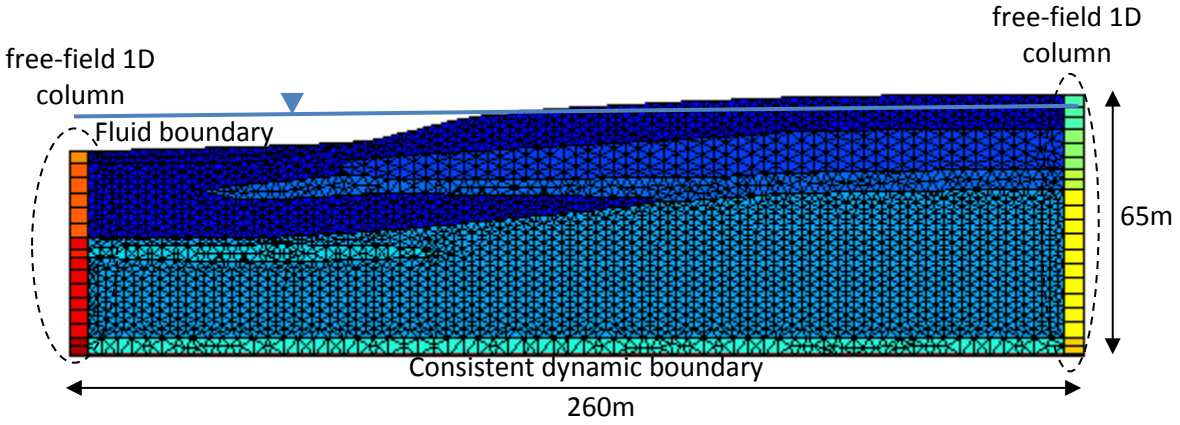

Figure 6. Finite Element Model

As the problem is not horizontally periodic, a standard tied approach (Zienkiewicz et al., 1988) is not appropriate for this case. To impose the free-field condition at the vertical edges, three approaches were investigated: (FEM-DOF) to impose displacements and pressures from a 1D dimensional propagation simulation; (FEM-Force) to impose equivalent lateral forces from free-field 1D column computations; (FEM-Column) which adds free-field columns at the lateral edges of the full 2D model. Approaches FEM-DOF and FEM-Force require two computations: first, the free-field 1D column must be solved and second, the equivalent displacements or forces must be imposed to the 2D model along the vertical edges. The FEM-Column approach has the advantage of requiring a single computation.

The finite element mesh that was used is shown in Figure 6, where each color corresponds to different material properties. For the FEM-Column approach, the mesh includes free-field columns at both vertical ends, as Fig.6 shows. In the case of the FEM-DOF/Force approaches, the free-field columns are solved separately, and the 2D model includes only the displacements or forces applied on the vertical boundaries. This finite element mesh satisfies the condition of having at least eight nodes per wave-length up to 10 Hz. All calculations were carried out with the program GEFDyn. Once the initial stress state is computed, the seismic analysis is performed "around" the initial static situation, which corresponds to a dynamic disturbance analysis.

The Ecole Centrale Paris's (ECP) elasto-plastic multi-mechanism model (Hujeux, 1985) was used to represent the sand behavior. The ability of this model to reproduce liquefaction has been highlighted in several studies (e.g. Lopez-Caballero and Modaressi, 2008, 2010; Sáez and Ledezma, 2014). Sands and silt models, consistent with the SPT/CPT data from the site, were selected from the authors' materials library.

To highlight the influence of the treatment of the vertical edges on the liquefaction-induced lateral-spreading, we selected the NS component from the Maule 2010 Earthquake record at Rapel station on rock. This station is located approximately 350 km north of Coronel, and the record has a duration of about 90s and a PGA of 0.2g. The effective motion at the bedrock level in this area was likely significantly stronger than the record in Rapel, but that's the closest reliable record on bedrock. Figure 7a displays the excess pore pressure ratio Ru contour plots at 80s for the three explored approaches. Only in the case of the FEM-Force approach liquefaction shows some discontinuity close to the toe of the slope. Despite these minor differences, results are qualitatively very similar.

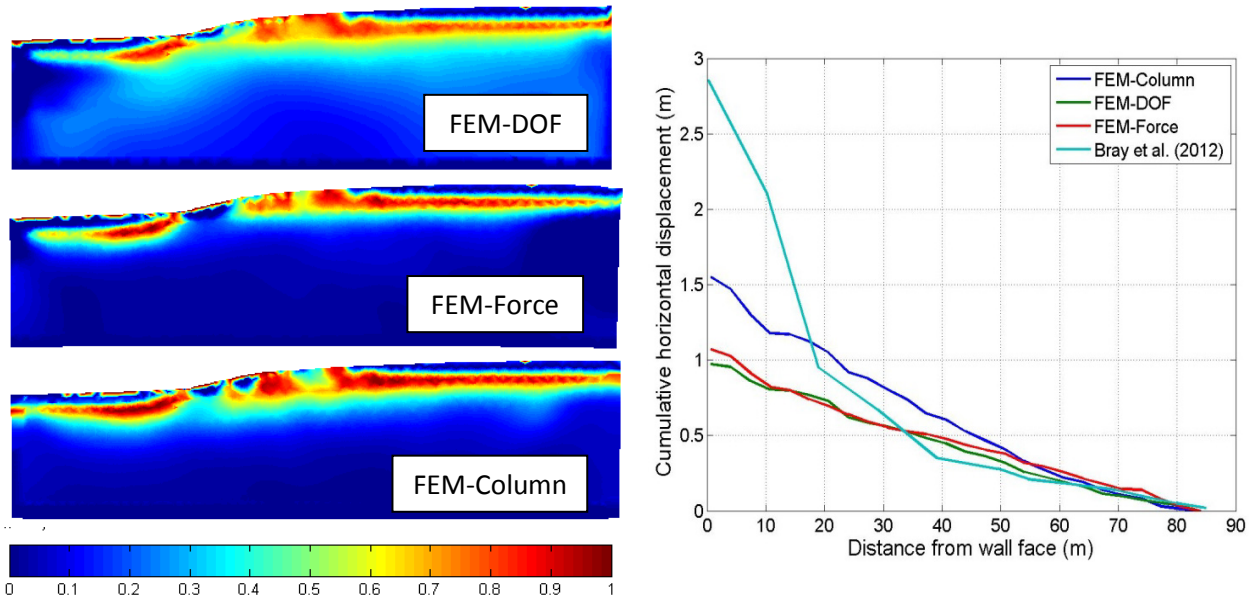

Figure 7. Boundary conditions benchmarking: (a) Pore pressure ratio Ru contour maps; (b) cumulated horizontal displacement

For a more quantitative comparison, Figure 7b shows the cumulative horizontal displacements measured across the projection of the line measured by Bray et al. (2012) over the section considered for modeling. In terms of maximum values, the FEM-Column approach provided the closest value when compared against field measurements (about 57% less than the total cumulative horizontal displacement). Large displacement increment that takes place in the first 20m is not properly captured by the numerical model. It is likely that the wide cracks observed in the field cannot be reproduced by a continuous modeling strategy such as FEM.

Conclusions

In the present study, an extensive survey including geophysical methods, SPT, and CPT soundings was conducted to characterize the site of Caleta Lo Rojas in Coronel city, where large seismically-induced lateral spreading was reported for the Maule 2010 earthquake. The information indicates that the site is characterized by a steep slope of about 11% along approximately 90m. The shallowest soil layer is characterized by 7m of low-density clean sand, followed by about 5m of clayed sand. Below this level, the high fines content (larger than 50%) defines a boundary driving lateral-spreading. Based on this information advanced modeling

approaches were applied to reproduce the observed post-seismic displacements.

The results obtained using the FEM-Column approach are probably accurate enough for design purposes. A laboratory testing program is currently being conducted using samples from ST-1. Based on these laboratory results, constitutive models will be recalibrated to improve the FEM results. Also, the simultaneous inclusion of the vertical component of the record will be considered in future stages of this investigation.

Acknowledgments

Support for this work was provided by the Comisión Nacional de Investigación Científica y Tecnológica de Chile (CONICYT) under Award No. USA2012-0007.

References

Aki, K., 1957. Space and time spectra of stationary stochastic waves, with spectral reference to microtremors, *Bull. Earthq. Res. Inst*. **35**, 415–456.

Bray, J., Rollins, K., Hutchinson, T., Verdugo, R., Ledezma, C., Mylonakis, G., Assimaki, D., Montalva, G., Arduino, P., Olson, M., Kayen, R., Hashash, Y. M. A., Candia, G., 2012. Effects of Ground Failure on Buildings, Ports, and Industrial Facilities. *Earthquake Spectra*. **28**, 97-118.

Bray, J., Sancio, R., 2006. Assessment of the Liquefaction Susceptibility of Fine-Grained Soils. *Journal of geotechnical and geoenvironmental engineering*. **132**(9), 1165-1177.

Hayashi, K., 2008. *Development of the Surface-wave Methods and its Application to Site Investigation*. Ph.D Dissertation, Kyoto University.

Hujeux, J.C., 1985. Une loi de comportement pour le chargement cyclique des sols. *Génie Parasismique*, Presse ENPC. 287-302. (in French).

Lacoss, R. T., Kelly, E. J., Toksöz, M. N., 1969. Estimation of seismic noise structure using arrays. *Geophysics*. **34**(1), 21-38.

Lopez-Caballero, F., Modaressi, A., 2008. Numerical simulation of liquefaction effects on seismic SSI. *Soil Dynamics and Earthquake Engineering*. **28**, 85-98.

Lopez-Caballero, F., Modaressi, A., 2010. Assessment of variability and uncertainties effects on the seismic response of a liquefiable soil profile. *Soil Dynamics and Earthquake Engineering*. **7**, 600-613.

Nakamura, Y., 1989. A method for dynamic characteristics estimation of subsurface using microtremor on the ground surface. *Railway Technical Research Institute*. **30**, 25-30.

Park, C. B., Miller, R. D., Xia, J., 1999. Multichannel analysis of surface waves. *Geophysics*. **64**(3), 800-808.

Sáez, E., Ledezma, C., 2014. Liquefaction mitigation using secant piles wall under a large water tank. *Soil Liquefaction during Recent Large-Scale Earthquakes*, CRC Press.

Wathelet, M., Jongmans, D., Ohrnberger, M., Bonnefoy-Claudet, S., 2008. Array performances for ambient vibrations on a shallow structure and consequences over Vs inversion. *Journal of Seismology*. **12**(1),1-19.

Youd, T. L., Idriss, I. M., Andrus, R. D, et al., 2001. Liquefaction Resistance of Soils: Summary Report from the 1996 NCEER and 1998 NCEER/NSF Workshops on Evaluation of Liquefaction Resistance of Soils. *Journal of Geotechnical and Geoenvironmental Engineering* ASCE. **127**(10), 817-833.

Zienkiewicz, O., Bicanic, N., Shen, F., 1988. Earthquake input definition and transmitting boundary conditions. In: *Advances in Computational Nonlineal Mechanics*. 109-138.

Zienkiewicz, O., Shiomi, T., 1984. Dynamic behaviour of saturated porous media: the generalized Biot formulation and its numerical solution. *International Journal of Numerical and Analytical Methods in Geomechanics*. **8**, 71-96.